Long-term operation of a reverse Brayton heat pump coupled to a packed-bed thermal energy storage system under stochastic scheduling

Chen Liu[a], Guido Francesco Frate[b], Lorenzo Ferrari[c] and Umberto Desideri[d]

[a] *University of Pisa, Department of Energy, Systems, Territory and Constructions Engineering, Pisa, Italy, chen.liu@phd.unipi.it, CA*

[b] *University of Pisa, Department of Energy, Systems, Territory and Constructions Engineering, Pisa, Italy, guido.frate@unipi.it*

[c] *University of Pisa, Department of Energy, Systems, Territory and Constructions Engineering, Pisa, Italy, lorenzo.ferrari@unipi.it*

[d] *University of Pisa, Department of Energy, Systems, Territory and Constructions Engineering, Pisa, Italy, umberto.desideri@unipi.it*

Abstract:

This study investigates the control feasibility and long-term operating characteristics of a reverse Brayton heat pump coupled with a packed-bed thermal energy storage system under stochastic scheduling, in order to support flexible thermal energy storage operation under fluctuating conditions. A coupled thermodynamic model is developed, and a feedback control strategy is proposed in which the packed-bed-side mass flow rate is adjusted to regulate the charging inlet temperature. Under a 30-day stochastic operating schedule, the system is evaluated in terms of charging/discharging completion, state-of-charge (SOC) evolution, round-trip efficiency, and average output performance. The results show that the proposed control strategy can effectively maintain the charging inlet temperature near its target value. Although the rise in turbine inlet temperature during charging gradually drives the heat pump away from its rated operating condition and reduces the coefficient of performance (COP), this effect mainly occurs within individual charging processes and does not accumulate from day to day. Over the 30-day simulation, the charging and discharging completion ratios range from 70% to 100% and from 59% to 100%, respectively. The end-of-charging SOC is mostly concentrated between 80% and 90%, whereas the end-of-discharging SOC is generally reduced to 5%–8%. In addition, the round-trip efficiency is mainly distributed between 80% and 85%, while the daily mean discharging outlet temperature and the daily charging COP remain around 256.0 °C and 1.54, respectively, without any evident long-term decline at the daily scale. Overall, stochastic scheduling mainly affects the cycle-to-cycle matching between charging and discharging rather than causing cumulative performance degradation. The proposed control strategy can therefore support relatively stable long-term operation under stochastic operating conditions.

Keywords:

Packed bed; Reverse Brayton heat pump; Stochastic scheduling; Long-term operation; Feedback control.

1. Introduction

1.1. Background and state of the art

With the increasing penetration of renewable energy and the ongoing electrification of end-use sectors, the mismatch between fluctuating electricity supply and industrial heat demand has become increasingly prominent. In 2024, renewable energy contributed nearly one-third of global electricity generation, but accounted for only slightly more than 8% of total global energy demand [1], indicating that substantial decarbonisation pressure remains in end-use sectors. Meanwhile, the temperature range of 100–300 °C represents a typical medium-temperature heat demand interval in industrial processes and accounts for approximately 37% of European industrial process heat demand [2, 3]. Therefore, thermal energy storage (TES) systems and their flexible operation for this temperature range are of clear practical relevance.

Among various TES technologies, packed-bed (PB) sensible heat storage has attracted considerable attention because of its simple structure, low-cost storage medium, compatibility with air as the heat transfer fluid, and applicability over a wide temperature range [4, 5]. In recent years, research has mainly focused on the optimisation of storage materials and bed configurations, as well as their effects on heat transfer behaviour

and overall thermal performance [6-9]. Although PB systems offer low cost and good engineering scalability, their performance remains strongly influenced by thermal front evolution, pressure drop, and operating conditions [10, 11].

However, the PB mainly serves as a unit for thermal energy storage and release, and cannot actively upgrade low-grade heat to a temperature level suitable for charging. Therefore, introducing a heat pump as the active heat source during charging offers a clear advantage. The reverse Brayton heat pump operates with an air-based sensible heating cycle, which is compatible with air-based packed-bed thermal storage. Once coupled, the system can upgrade low-grade thermal energy during charging and release the stored heat during discharging, thereby combining active charging capability with thermal energy shifting [12].

Pérez-Gallego et al. [13] examined the coupling performance between PB storage and Brayton cycles from a modelling perspective under prescribed charge–storage–discharge conditions, with particular attention to storage efficiency and Brayton-cycle efficiency in single and successive cycles. Wang et al. [14] investigated the operation modes and cyclic transient behaviour of PB TES arrays in a Joule–Brayton pumped heat electricity storage system under fixed charge/discharge durations and predefined operating modes, focusing on round-trip efficiency and delivery power variation. Ameen et al. [15] validated the cyclic operating performance of a PB system coupled with a closed Brayton cycle at the demonstrator scale under prescribed cycling conditions, showing that PB behaviour and the initial transient state can significantly affect overall system performance. Overall, existing studies have progressed from coupling-performance analysis to operation-mode assessment and demonstrator-scale validation. However, their primary focus remains on system-level energy recovery, electricity round-trip efficiency, and power output, while the operating conditions considered are still mostly based on prescribed charge/discharge cycles. By contrast, for reverse Brayton heat pump–packed bed systems intended for thermal output, existing research has paid relatively limited attention to control response and long-term operating behaviour under irregular operating conditions. For such systems, there is a strong coupling between the HP side and the PB side during operation, and the overall performance depends on the matching among charging control, the evolution of the storage state, and the subsequent discharging process. Therefore, performance evaluation based only on design-point or regular operating conditions is insufficient to fully reflect the control feasibility and operational stability of the system under practical operating conditions.

1.2. Objectives and contributions

Motivated by the above research gap, this study aims to investigate the control feasibility and long-term operating characteristics of a reverse Brayton heat pump coupled with a packed-bed thermal energy storage system under stochastic scheduling. Specifically, a coupled system model is established, and a feedback control strategy is proposed in which the packed-bed-side mass flow rate is adjusted to regulate the charging inlet temperature. Under a 30-day stochastic operating schedule, the study focuses on the completion of charging and discharging processes, the evolution of the storage state, the round-trip efficiency, and the average output performance of the system. These analyses provide useful insights for the control and stable operation of reverse Brayton heat pump–packed bed systems under irregular operating conditions.

2. Methodology

2.1. System description

As illustrated in Figure 1, the system comprises two main subsystems: a reverse Brayton cycle heat pump (HP) and a PBTES unit, coupled thermally through a heat exchanger (HX).

The HP consists of a compressor (C), a turbine (T), and HX. The working fluid (air) enters the compressor at state 1 at ambient temperature and low pressure, and is compressed to state 2 with elevated temperature and pressure. It then transfers heat to the PB side through the HX and cools to state 3, before expanding through the turbine to state 4 at a lower temperature. The cycle operates as an open cycle on the low-temperature side: the turbine exhaust at state 4 is discharged to the environment, and ambient air is drawn into the compressor at state 1. The compressor operates at variable speed to regulate the mass flow rate on the HP side ($\dot{m}_{HP}$).

The PB side operates through two separate flow circuits for charging and discharging, with each daily cycle divided into four sequential phases: charging, idle after charging, discharging, and idle after discharging. During charging, a variable-speed fan circulates air through a closed loop: air is heated to charging inlet temperature ($T_{ch,in}$) by the heat exchanger and enters the PB from the top, transferring thermal energy to the solid particles before cooling to charging outlet temperature ($T_{ch,out}$) and returning to the HX from the bottom. The fan speed is continuously adjusted by the control strategy to regulate the mass flow rate on the PB side ($\dot{m}_{PB}$). During the idle period, the fan is switched off and the bed undergoes internal temperature redistribution under zero-flow conditions. During discharging, ambient-temperature air is supplied at a fixed rated $\dot{m}_{PB}$ from

the bottom of the bed, absorbs the stored thermal energy, and exits from the top at discharging outlet temperature ($T_{dis,out}$) to a downstream process, the details of which are beyond the scope of this study. Following discharging, the system enters the second idle period, which persists until the start of the next day's charging phase.

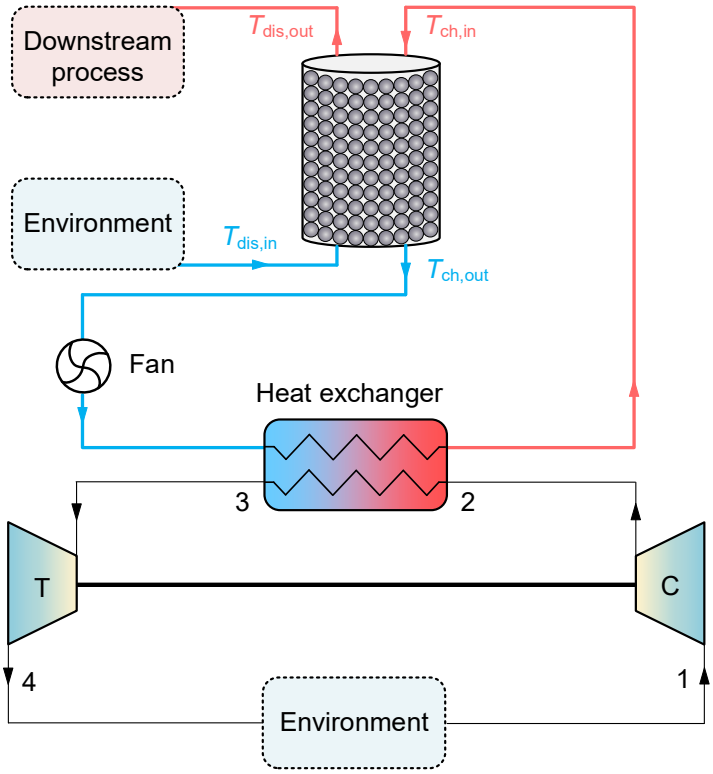

Figure. 1. *Schematic of the reverse Brayton heat pump coupled packed bed thermal energy storage system.*

2.2. Mathematical models

2.2.1. Reverse Brayton cycle model

The reverse Brayton cycle is modelled under quasi-steady-state conditions, where thermodynamic equilibrium is assumed at each simulation time step. The working fluid is air, with thermodynamic properties evaluated at each state point using CoolProp V6.6.0 [16]. The isentropic efficiencies of the compressor (η_c) and turbine (η_t) are assumed constant and independent of the $\dot{m}$. The HX is assumed to have a fixed thermal effectiveness, accounting for minor heat losses.

The actual enthalpy (h) at the compressor outlet (state 2) and turbine outlet (state 4) are obtained by correcting the isentropic values with the respective efficiencies:

$$h_2 = h_1 + \left(h_{2s} - h_1\right)/\eta_c \tag{1}$$

$$h_4 = h_3 - \eta_t \cdot \left(h_3 - h_{4s}\right) \tag{2}$$

During operation, state 3 is governed by a pinch constraint at the HX (ΔT_{PP}):

$$T_3 = T_{ch,out} + \Delta T_{PP} \tag{3}$$

The $\dot{m}_{HP}$ varies with the HX outlet conditions, with the choke coefficient (C_{choke}) being a constant calibrated at the design point:

$$\dot{m}_{HP} = C_{choke} \cdot p_2 / \sqrt{T_3} \tag{4}$$

The heat rejected by the HP and the thermal power delivered to the PB side are then:

$$Q_{HP} = \dot{m}_{HP} \cdot \left(h_2 - h_3\right) \tag{5}$$

$$Q_{HX} = \eta_{HX} \cdot Q_{HP} \tag{6}$$

The PB charging inlet temperature is determined from an energy balance on the PB-side air:

$$h_{\mathrm{ch,in}} = h_{\mathrm{PB,out}} + Q_{\mathrm{HX}} / \dot{m}_{\mathrm{PB}} \tag{7}$$

The coefficient of performance (COP) is defined as:

$$\mathrm{COP} = Q_{\mathrm{HP}} \Big/ \left\{ \dot{m}_{\mathrm{HP}} \cdot \left[\left(h_2 - h_1 \right) - \left(h_3 - h_4 \right) \right] \right\} \tag{8}$$

2.2.2. Packed bed model

Solid and gas properties are assumed to vary only along the axial direction, and the kinetic and potential energy of the airflow are also considered negligible. Based on these assumptions, the temperature evolution of both phases is described by the one-dimensional two-phase Schumann model [17]. The detailed formulations for related model parameters are provided in our previous work [18]. Based on their material properties and cost-effectiveness, air, and basalt are selected as the fluid and storage medium in the PB system.

$$\varepsilon \left(\rho c_{\mathrm{p}} \right)_{\mathrm{f}} \frac{\partial T_{\mathrm{f}}}{\partial t} + \left(\rho c_{\mathrm{p}} \right)_{\mathrm{f}} v_{\mathrm{f}} \frac{\partial T_{\mathrm{f}}}{\partial z} = \frac{\partial}{\partial z} \left(k_{\mathrm{f}} \frac{\partial T_{\mathrm{f}}}{\partial z} \right) + \alpha_{\mathrm{eff}} A_{\mathrm{p}} \left(T_{\mathrm{s}} - T_{\mathrm{f}} \right) + U_{\mathrm{w}} A_{\mathrm{w}} \left(T_{\mathrm{amb}} - T_{\mathrm{f}} \right) \tag{9}$$

$$\left(1 - \varepsilon \right) \left(\rho c_{\mathrm{p}} \right)_{\mathrm{s}} \frac{\partial T_s}{\partial t} = \frac{\partial}{\partial z} \left(k_{\mathrm{eff,s}} \frac{\partial T_s}{\partial z} \right) + \alpha_{\mathrm{eff}} A_{\mathrm{p}} \left(T_{\mathrm{f}} - T_{\mathrm{s}} \right) \tag{10}$$

The following performance metrics are used to evaluate the system over the 30-day simulation.

The state of charge (SOC) of the PB is defined as the ratio of the current stored thermal energy to the maximum storage capacity, evaluated relative to a reference temperature (T_{ref}):

$$\mathrm{SOC} = \frac{\int_0^H \rho_s \left(1 - \varepsilon \right) A_{\mathrm{c}} c_{\mathrm{p,s}} \left(T_{\mathrm{s}} \left(z,t \right) - T_{\mathrm{ref}} \right) dz}{m_{\mathrm{s}} c_{\mathrm{p,s}} \left(T_{\mathrm{ch,in,target}} - T_{\mathrm{ref}} \right)} \tag{11}$$

where A_{c} is the cross-sectional area of the bed. The SOC is evaluated at the end of charging ($\mathrm{SOC_{ch}}$) and at the end of discharging ($\mathrm{SOC_{dis}}$), characterising the degree of charge and the residual stored energy respectively.

The round-trip efficiency (η_{RT}) is defined as the ratio of the thermal energy discharged to the thermal energy charged over a daily cycle [19]:

$$\eta_{\mathrm{RT}} = \frac{\int \dot{m}_{\mathrm{PB}} \left(h_{\mathrm{dis,out}} - h_{\mathrm{dis,in}} \right) dt}{\int \dot{m}_{\mathrm{PB}} \left(h_{\mathrm{ch,in}} - h_{\mathrm{ch,out}} \right) dt} \tag{12}$$

2.3. Control strategy

The daily schedule is determined by an external file incorporating stochastic variations to simulate real-world load fluctuations, with charging beginning at 00:00 and discharging fixed at 12:00 each day. At the end of each day, $\dot{m}_{\mathrm{PB}}$ is reset to its rated value as the initial condition for the next day's charging. Day 21 is designated as a full idle day to examine the effect of a severe disturbance on subsequent system performance.

The objective of the charging control is to maintain the $T_{\mathrm{ch,in}}$ at a target value ($T_{\mathrm{ch,in,target}}$). $T_{\mathrm{ch,in}}$ is jointly determined by the coupling between the HP and PB sides: the compressor operates at a fixed pressure ratio, by adjusting its rotational speed, continuously supplying heat to the HX, while $T_{\mathrm{ch,in}}$ depends on the balance between the heat delivered to the PB-side air and its $\dot{m}_{\mathrm{PB}}$. The PB-side fan $\dot{m}_{\mathrm{PB}}$ is therefore selected as the control variable — increasing $\dot{m}_{\mathrm{PB}}$ lowers $T_{\mathrm{ch,in}}$, while decreasing $\dot{m}_{\mathrm{PB}}$ raises it. The HP-side $\dot{m}_{\mathrm{HP}}$ varies passively with the HX outlet temperature T_3 and is not actively controlled, but must remain within its permitted range. The control layout is illustrated in Figure 2, indicating the controlled variable ($T_{\mathrm{ch,in}}$), manipulated variable ($\dot{m}_{\mathrm{PB}}$), measured variable ($T_{\mathrm{ch,out}}$), and monitored variables ($\dot{m}_{\mathrm{HP}}$, T_4).

At each time step, $T_{\mathrm{ch,in}}$ is first estimated using the current bed $T_{\mathrm{ch,out}}$ and $\dot{m}_{\mathrm{PB}}$; $\dot{m}_{\mathrm{PB}}$ is then adjusted based on the deviation between the estimated and target values; and the updated $\dot{m}_{\mathrm{PB}}$ is used to compute the actual $T_{\mathrm{ch,in}}$ and HP state for that time step. The $\dot{m}_{\mathrm{PB}}$ adjustment follows a proportional dead-band feedback control scheme. In contrast, during discharging, no active control is applied and the fan operates at the rated mass flow rate ($\dot{m}_{\mathrm{PB,rated}}$).

Charging or discharging is immediately terminated when any of the following conditions is met:

- The turbine outlet temperature T_4 reaches the compressor inlet temperature T_1, indicating HP cycle degradation (charging only);
- The $\dot{m}_{PB}$ or $\dot{m}_{HP}$ exceeds its permitted range (charging only);
- The difference between the initial and final solid temperatures at the outlet ($\Delta T_{ch/dis,s,out}$) reaches the predetermined threshold of 100 °C, preventing overcharging or overdischarging;
- The scheduled duration is reached.

The control parameters and system design values used in the simulation are summarised in Table 1, and the full control logic is illustrated in Figure 3.

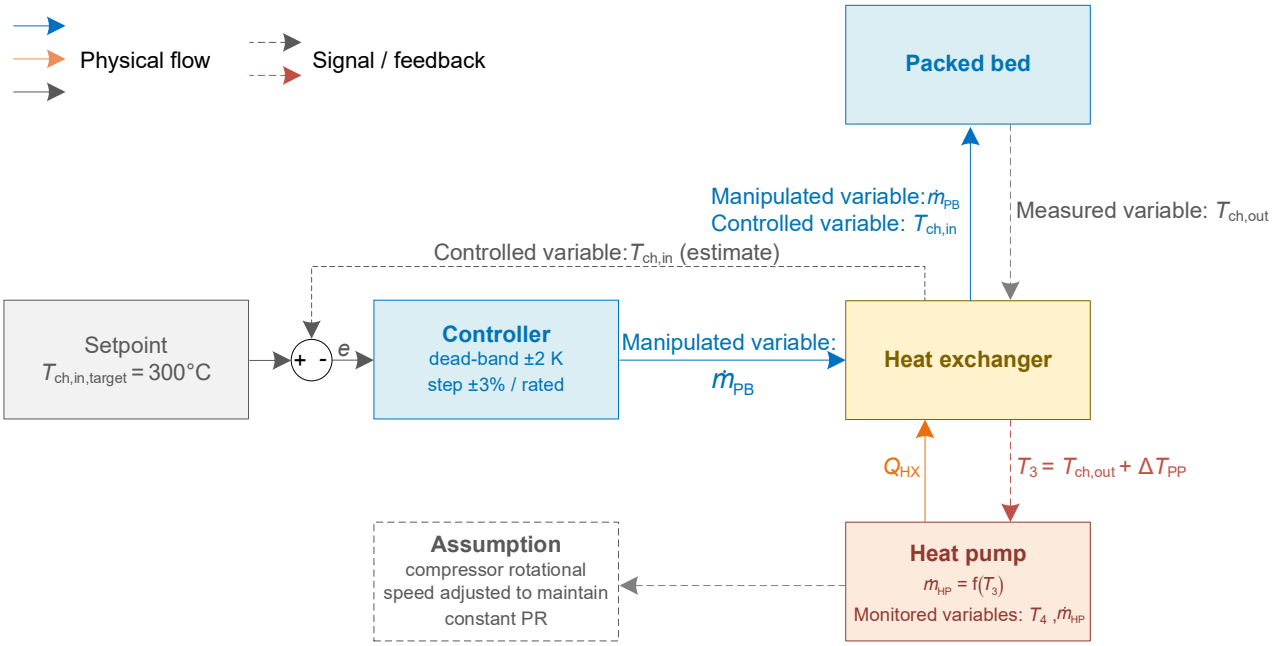

Figure. 2. *Control block diagram of the charging control strategy, indicating the controlled variable, manipulated variable, measured variable, and monitored variables.*

Table 1. *System parameters used in the simulation.*

Parameter	Symbol	Value	Unit
Reverse Brayton cycle heat pump			
Rated thermal output	Q_{HP}	250	kW
Compressor inlet pressure	p_1	1.05	MPa
Pressure ratio	PR	12.51	-
Ambient temperature	T_0	15	°C
Rated compressor outlet temperature	T_2	300	°C
Rated turbine inlet temperature	T_3	35	°C
Compressor isentropic efficiency	η_c	0.85	-
Turbine isentropic efficiency	η_t	0.9	-
Heat exchanger efficiency	η_{HX}	0.98	-
Pinch temperature difference	ΔT_{PP}	20	K
Rated COP	COP_{rated}	1.55	-
Rated mass flow rate	$\dot{m}_{HP,rated}$	0.72	kg/s
Mass flow rate range	$[\dot{m}_{HP,min}, \dot{m}_{HP,max}]$	$[0.8\times\dot{m}_{HP,rated}, 1.2\times\dot{m}_{HP,rated}]$	kg/s
Packed bed			
Bed height	H	3.75	m
Inner and outer diameter	D_{in} / D_{out}	1.87 /1.97	m
Particle diameter	D_p	0.01	m
Void ratio	ε	0.4	-
Rated mass flow rate	$\dot{m}_{PB,rated}$	0.84	kg/s
Mass flow rate range	$[\dot{m}_{PB,min}, \dot{m}_{PB,max}]$	$[0.8\times\dot{m}_{PB,rated}, 1.2\times\dot{m}_{PB,rated}]$	kg/s
Initial bed temperature	T_{ini}	15	°C
Charging inlet target temperature	$T_{ch,in,target}$	300	°C
Discharging inlet temperature	$T_{dis,in}$	15	°C
Rated charging time	$t_{c,rated}$	6	h

Parameter	Symbol	Value	Unit
Temperature deviation threshold	$\Delta T_{ch/dis,s,out}$	100	°C
Dead-band tolerance	tol	2	K
Flow rate adjustment step	β	0.03	%

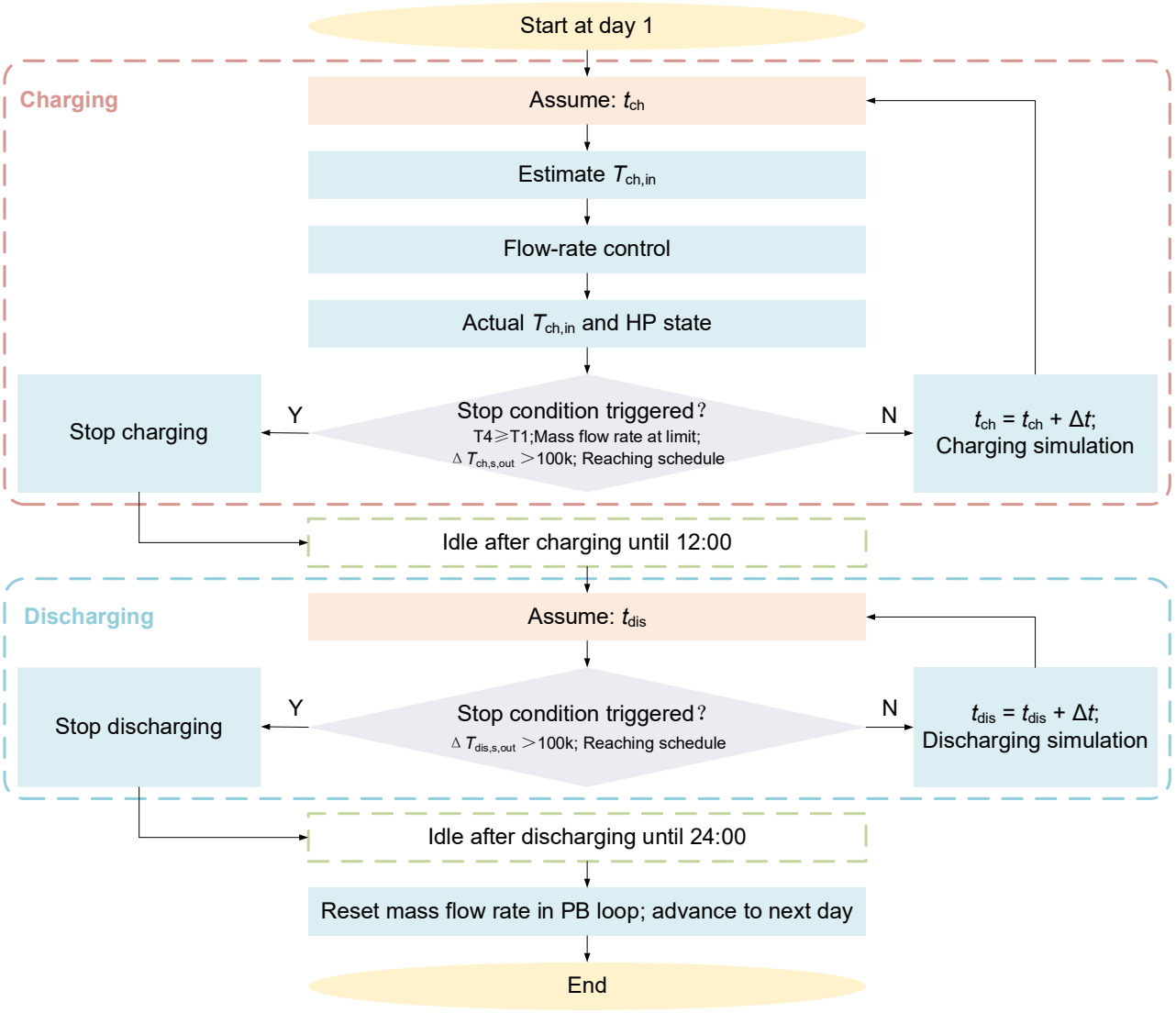

Figure. 3. *Flowchart of the daily operation and control strategy.*

3. Results and discussion

Figure 4 presents the solid-phase temperature profiles along the normalised bed length (z/H) at six equally spaced time instants during each of the four operational phases on a representative day (Day 1).

During charging in Figure 4(a), hot air enters the bed from the top (z/H = 1) and a thermal front propagates progressively towards the bottom. By the end of charging, the upper portion of the bed approaches the target temperature of 300°C, while the lowest 15% remains at the initial temperature of 15°C, indicating that the thermal front has not yet reached the bed outlet. Charging terminates upon reaching the scheduled duration without triggering any early-stop condition, reflecting the incomplete charging of the bed on Day 1 due to the cold-start initial condition.

During the first idle period in Figure 4(b), interphase heat exchange, axial effective conduction, and wall heat losses act together to reduce internal temperature gradients and homogenise the temperature distribution, with the high-temperature region at the bed top experiencing a temperature drop of approximately 20 K.

During discharging in Figure 4(c), cold air enters from the bottom (z/H = 0) and extracts stored thermal energy as it flows upward. The solid temperature at the bed outlet rises continuously until the temperature increase

relative to the start of discharging exceeds the threshold $\Delta T_{dis,s,out}$ = 100 K, at which point discharging is terminated early to prevent over-discharging and maintain the quality of the downstream heat output.

During the second idle period in Figure 4(d), the lower portion of the bed remains near the initial temperature following discharging. while the upper region retains residual thermal energy. This residual heat is carried over as the initial condition for the next day's charging cycle.

The single-day temperature profiles presented above reveal the thermodynamic behaviour of the system under typical operating conditions. To further assess the robustness of the control strategy under long-term stochastic scheduling, Figure 5 presents the time evolution of key operating variables across four representative days (Day 1, 8, 15, and 22).

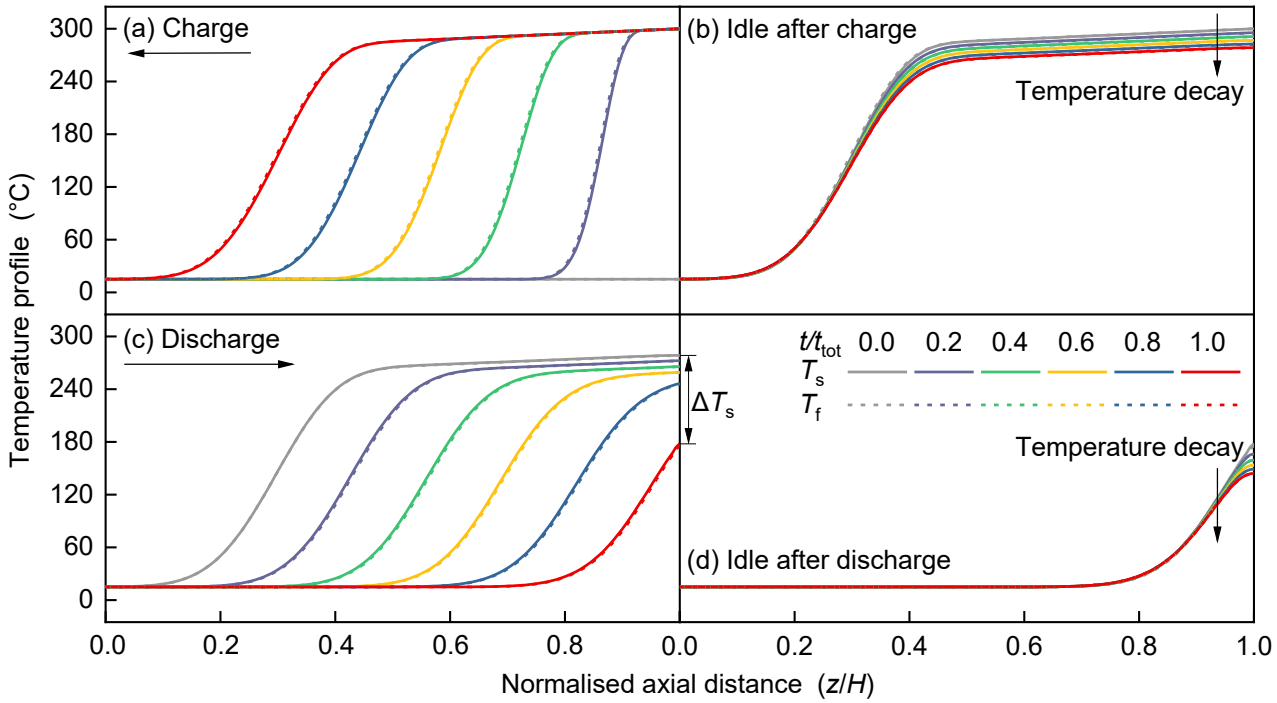

Figure. 4. *Packed bed temperature profiles during one representative day (Day 1): a) charge, b) idle after charge, c) discharge, d) idle after discharge.*

During the early charging phase, $T_{ch,out}$ remains at 15°C, while $T_{ch,in}$ is stably maintained near the target value of 300°C. Both $\dot{m}_{PB}$ and $\dot{m}_{HP}$ are at their rated values, and the COP is at its rated value of 1.55. The system operates at its rated condition and no control intervention is required. As charging progresses, $T_{ch,out}$ rises gradually, causing $T_{ch,in}$ to deviate from the target. The controller intervenes by adjusting $\dot{m}_{PB}$, which exhibits an alternating oscillatory pattern due to the dead-band tolerance, with $T_{ch,in}$ showing corresponding periodic fluctuations in Figures 5(a) and (b). On Day 1 and Day 15, the scheduled charging duration is relatively short, $T_{ch,out}$ does not rise significantly before charging ends, and control intervention is limited; $T_{ch,out}$ and $\dot{m}_{HP}$ remain virtually unchanged throughout, and the system operates continuously within the high-efficiency region. On Day 8 and Day 22, the longer scheduled duration allows $T_{ch,out}$ to rise more substantially, resulting in prolonged control intervention.

During discharging, $\dot{m}_{PB}$ operates at its rated value and $T_{dis,out}$ decreases monotonically throughout with no stable phase. Despite variability in daily conditions, $T_{dis,out}$ remains within a comparable range at the onset of discharging across all four days, although it is consistently slightly lower than 300°C due to thermal relaxation and heat loss during the intermediate idle period.

Unlike the active regulation of $\dot{m}_{PB}$, $\dot{m}_{HP}$ decreases passively and monotonically as T_3 rises in Figure 5(b), with a maximum reduction of approximately 14% observed on Day 22, from the rated value of 0.72 kg/s to approximately 0.62 kg/s. The sustained increase in T_3 simultaneously drives the HP operating point away from its rated condition, causing the COP to decline from its design value of 1.55 to approximately 1.40 in Figure 5(c), reflecting progressive performance degradation of the HP during extended charging.

These results demonstrate that the control strategy effectively suppresses $T_{ch,in}$ deviations through active regulation of $\dot{m}_{PB}$. However, the passive drift of the HP operating condition as charging progresses leads to an inevitable decline in COP, which represents the primary performance penalty associated with extended charging durations.

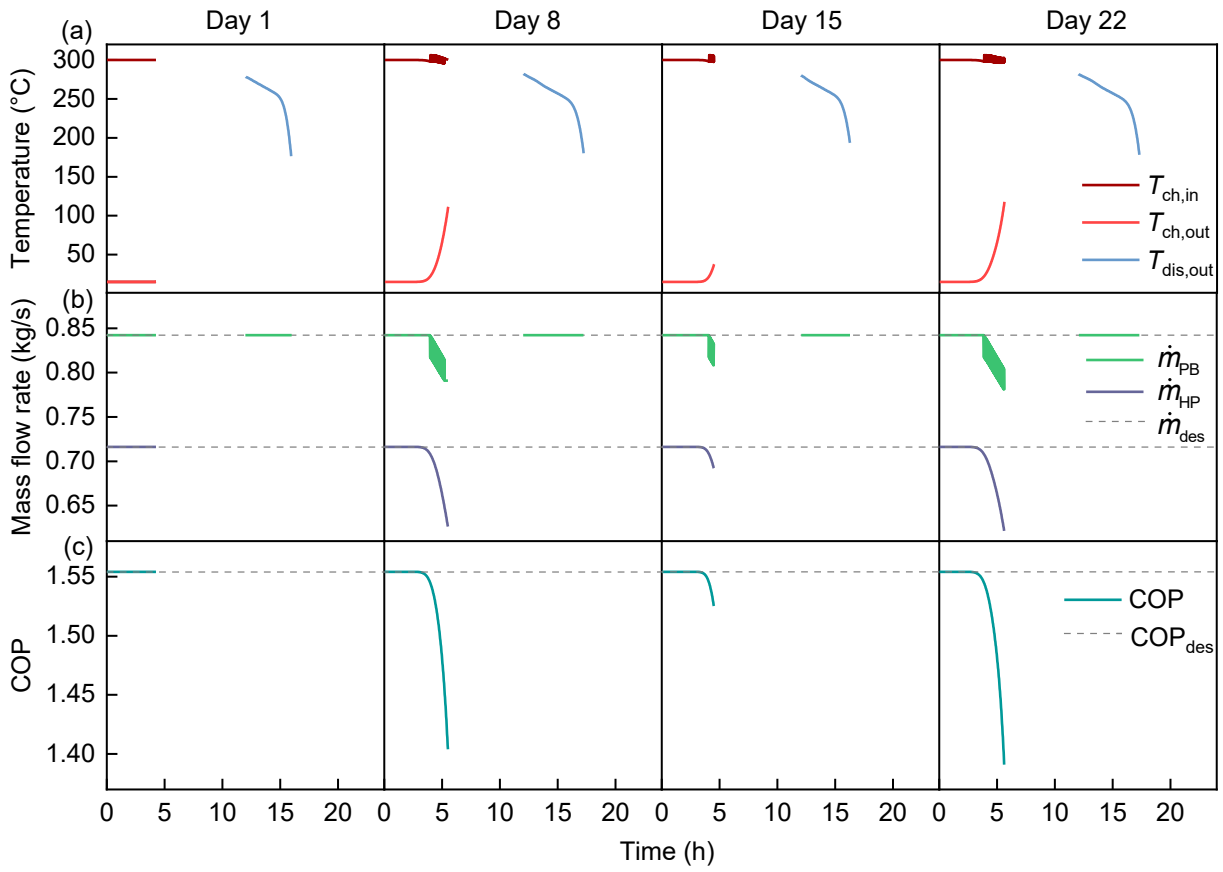

Figure. 5. *Time evolution of key operating variables during four representative days (Day 1, 8, 15, 22): a) inlet and outlet temperature, b) mass flow rate, c) COP.*

Figure 6 presents the scheduled and actual durations alongside the completion ratios for charging and discharging across the full 30-day simulation period.

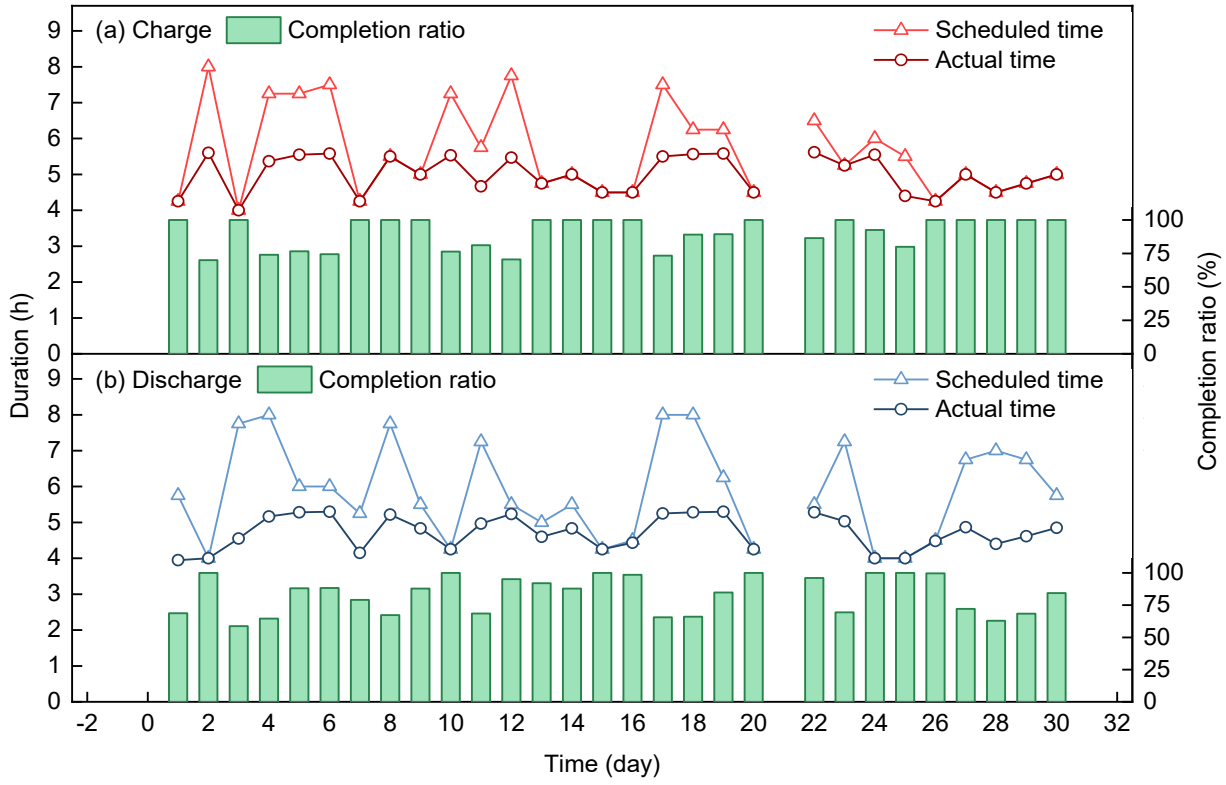

Figure. 6. *Scheduled and actual durations with completion ratios over the 30-day simulation period: a) charging, b) discharging.*

In terms of charging in Figure 6(a), approximately half of the days achieve a completion ratio of 100%, indicating that charging terminates upon reaching the scheduled duration. On the remaining days, the completion ratio ranges from 70% to 93%, with all cases terminated early due to the outlet temperature reaching the prescribed threshold.

According to the discharging in Figure 6(b), the completion ratio exhibits greater variability, ranging from 59% to 100%, with more than three-quarters of the days failing to reach the scheduled duration. This behavior is directly explained by the monotonically decreasing $T_{dis,out}$ observed in Figure 5(a). Unlike the charging phase, where a period of temperature stability exists, the $T_{dis,out}$ decreases continuously from the beginning, leading to earlier attainment of the cutoff threshold and thus shorter effective operating durations. Overall, across the 30-day simulation, both charging and discharging maintain consistent completion ratios from day to day, with no evident trend of progressive decline. This suggests that the system can sustain stable operation under stochastic load variations.

Figure 7 presents the SOC and η_{RT} of the PB over the 30-day simulation period. As shown in Figure 7(a), the end-of-charging SOC ranges from 68% to 90%, with most values concentrated between 80% and 90%, whereas the end-of-discharging SOC is mostly within 5%–8%, with only a few days increasing to 18%–22%. This indicates that, under stochastic scheduling, the PB generally reaches a high SOC at the end of charging and returns to a low SOC at the end of most discharging cycles, without showing any evident long-term drift.

On a few days, the residual SOC at the end of discharging is noticeably higher, particularly on Days 2, 10, and 24, for which the end-of-discharging SOC is approximately 22.0%, 18.3%, and 21.9%, respectively. These three days also correspond to relatively low η_{RT} of 65.5%, 70.4%, and 66.2%, indicating that the lower η_{RT} is closely associated with high residual energy remaining at the end of the cycle. Since these cycles store a considerable amount of thermal energy during charging while still retaining a high SOC after discharging, their heat recovery ratio is correspondingly lower.

By contrast, high η_{RT} are observed on Days 3, 11, and 26, reaching 96.2%, 93.3%, and 91.0%, respectively. The end-of-discharging SOC on these days is approximately 7.5%–9.8%, indicating low residual energy at the end of the cycle and thus a higher heat recovery ratio.

Overall, although both SOC and η_{RT} exhibit day-to-day fluctuations in Figure 7, their overall ranges remain stable, with no evident long-term drift or sustained decline. This demonstrates that, under stochastic scheduling, the proposed control strategy is able to maintain relatively stable SOC and η_{RT}.

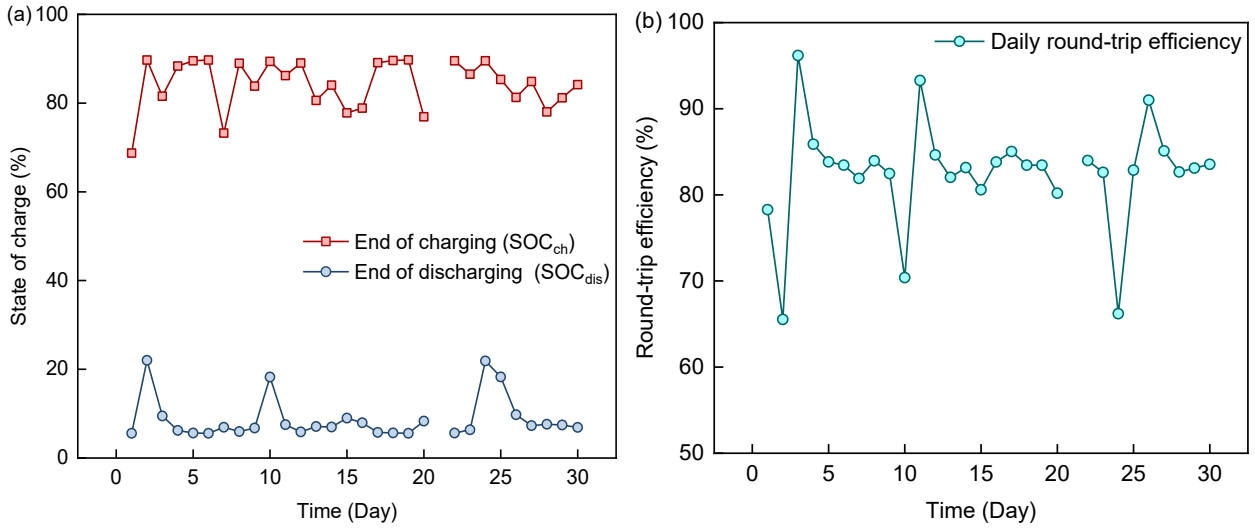

Figure. 7. *Daily packed bed performance over the 30-day simulation: a) state of charge at the end of charging and discharging; b) round-trip efficiency.*

Figure 8 shows the daily mean discharging outlet temperature and the daily charging COP over the 30-day simulation period. As shown in Figure 8(a), the mean discharging outlet temperature has an average value of 256.00 °C, with a standard deviation of 3.57 °C and a range of 15.80 °C. Although some day-to-day variation is observed, the overall distribution remains relatively concentrated, and no evident declining trend is found over time. This indicates that, under stochastic scheduling, the thermal output quality of the system remains generally stable without sustained deterioration.

Figure 8(b) shows that the daily charging COP has an average value of 1.54, with a standard deviation of only 0.01 and a range of 0.02, indicating very limited day-to-day variation. Combined with Figure 5(c), this suggests that the COP reduction mainly occurs within individual charging processes, as the rise in T_3 during the later charging stage drives the HP away from its rated operating point. However, this daily average masks the rapid COP drop that occurs near the end of some charging processes, because the low-COP period occupies only

a relatively short portion of the total charging duration. Thus, the daily average is dominated by the long period during which the COP remains close to its rated value. Since the $\dot{m}_{HP}$ is re-initialized at the beginning of each day, this deviation does not accumulate from day to day, and therefore the daily charging COP does not exhibit any evident declining trend over the 30-day period. The remaining small day-to-day variations mainly reflect differences in charging duration and T_3 evolution among individual days.

Overall, although stochastic scheduling induces variations in the operating state of individual cycles, the daily thermal output quality and the charging performance remain stable at the daily scale. At the same time, the transient results reveal a rapid late-stage COP deterioration during extended charging, which is not fully captured by the daily average alone. This demonstrates that the proposed control strategy can sustain stable long-term operation under stochastic scheduling while also revealing a local performance limitation during the final stage of prolonged charging.

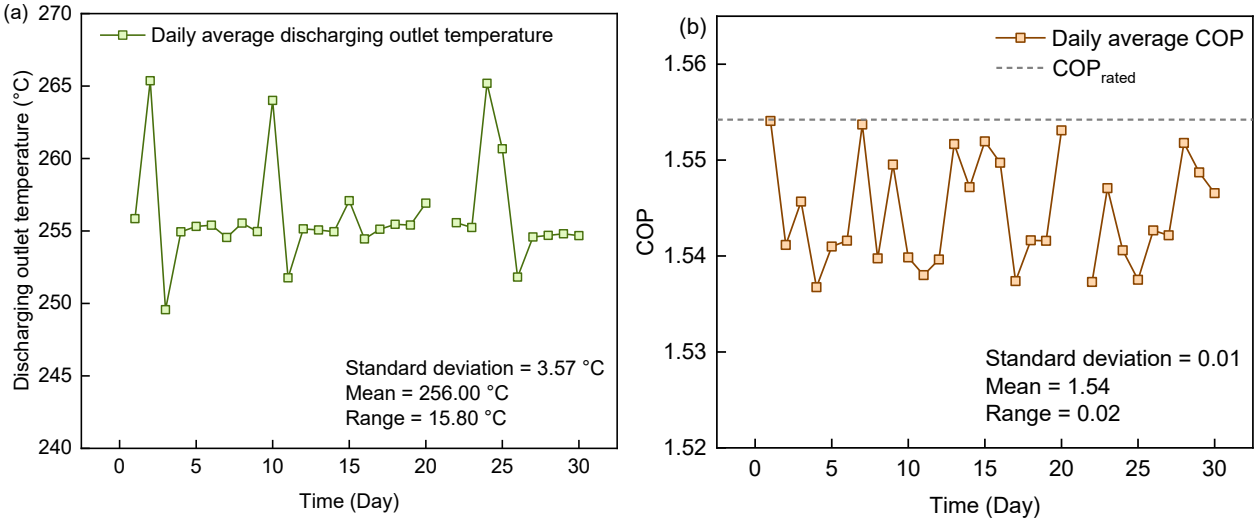

Figure. 8. *Daily system performance over the 30-day simulation: a) mean discharging outlet temperature; b) daily charging COP.*

4. Conclusion

This study developed a coupled thermodynamic model of a reverse Brayton cycle heat pump coupled packed-bed thermal energy storage system and proposed a feedback control strategy in which the packed-bed-side mass flow rate is regulated to maintain the charging inlet temperature under stochastic scheduling.

The results show that the proposed control strategy can effectively suppress charging temperature deviations and support stable long-term system operation. Over the 30-day simulation, the charging and discharging completion ratios range from 70% to 100% and from 59% to 100%, respectively, indicating that the scheduled operation is largely fulfilled under most conditions. The end-of-charging SOC is mostly concentrated between 80% and 90%, whereas the end-of-discharging SOC is generally reduced to 5%–8%, showing that the system can usually achieve a high charging level and release most of the stored thermal energy during discharging. Meanwhile, the round-trip efficiency is mainly distributed between 80% and 85%, and the daily mean discharging outlet temperature and daily charging COP remain around 256.0 °C and 1.54, respectively, without any evident long-term decline at the daily scale.

Overall, the main effect of stochastic scheduling lies in the variation of charge–discharge matching among individual cycles rather than cumulative performance degradation. Although the heat pump gradually deviates from its rated operating condition during extended charging, the associated COP reduction is mainly confined to individual charging processes and does not accumulate from day to day. These findings demonstrate that the proposed control strategy can support relatively stable long-term operation of the system under stochastic load conditions and provide useful guidance for its practical operation and control.

Acknowledgments

Chen Liu acknowledges the financial support from the China Scholarship Council (CSC), under grant number [CSC202308120015].

Nomenclature

Example:

A	area, m^2
c	specific heat capacity, J/(kg K)
C_{choke}	choke coefficient, kg/(s·Pa)·K^{1/2}
COP	coefficient of performance
D	diameter, m
h	specific enthalpy, kJ/kg
H	height, m
HX	heat exchanger
HP	reverse Brayton cycle heat pump
k	thermal conductivity, W/m K
m	mass, kg
$\dot{m}$	mass flow rate, kg/s
p	pressure, kPa
PB	packed bed
Q	thermal power, kW
SOC	state of charge
t	time, h
T	temperature, °C/K
TES	thermal energy storage
tol	dead-band tolerance, K
U	overall heat transfer coefficient through the wall, W/m^2 K
v	superficial velocity, m/s
z	vertical coordinate, m

Greek symbols

α	convective heat transfer coefficient, W/m^2 K
β	flow rate adjustment step, %
ε	void fraction
η	efficiency
ρ	density, kg/m^3

Subscripts and superscripts

1-4	state point
amb	ambient
C	compressor
c	cross-sectional
ch	charge
dis	discharge
eff	effective
f	fluid
in	inlet
out	outlet
p	particle
PP	pinch point
ref	reference
RT	round-trip
s	isentropic / solid
T	turbine
w	wall

References

[1] Energy Institute. Statistical Review of World Energy 2025 – Available at:< https://www.energyinst.org/statistical-review/energy-transition-tracker> [accessed 15.3.2026].

[2] Steinmann W.-D., Thermal energy storage for medium and high temperatures, Springer; 2022.

[3] Arpagaus C., Bless F., Uhlmann M., Schiffmann J., Bertsch S.S., High temperature heat pumps: Market overview, state of the art, research status, refrigerants, and application potentials, Energy, 152 (2018) 985-1010.

[4] Georgousis N., Diriken J., Speetjens M., Rindt C., Comprehensive review on packed-bed sensible heat storage systems, Journal of Energy Storage, 121 (2025) 116516.

[5] McTigue J.D., Markides C.N., White A.J., Performance response of packed-bed thermal storage to cycle duration perturbations, Journal of Energy Storage, 19 (2018) 379-392.

[6] Elouali A., Kousksou T., El Rhafiki T., Hamdaoui S., Mahdaoui M., Allouhi A., Zeraouli Y., Physical models for packed bed: Sensible heat storage systems, Journal of Energy Storage, 23 (2019) 69-78.

[7] Bindra H., Bueno P., Morris J.F., Shinnar R., Thermal analysis and exergy evaluation of packed bed thermal storage systems, Applied Thermal Engineering, 52 (2013) 255-263.

[8] Rusin K., Ochmann J., Bartela Ł., Rulik S., Stanek B., Jurczyk M., Waniczek S., Influence of geometrical dimensions and particle diameter on exergy performance of packed-bed thermal energy storage, Energy, 260 (2022) 125204.

[9] Wang Y., Wang Z., Yuan G., Control strategy effect on storage performance for packed-bed thermal energy storage, Solar Energy, 253 (2023) 73-84.

[10] Hernández-Jiménez F., Pérez-Álvarez R., López-Quesada G., García-Gutiérrez L.M., Effect of Biot number on the thermocline evolution of a packed bed TES system, Journal of Energy Storage, 110 (2025) 115272.

[11] Soprani S., Marongiu F., Christensen L., Alm O., Petersen K.D., Ulrich T., Engelbrecht K., Design and testing of a horizontal rock bed for high temperature thermal energy storage, Applied Energy, 251 (2019) 113345.

[12] Zhou J., Wu W., Bellamy L., Bishop D., Thermal energy storage–coupled heat pump systems: Review of configurations and modelling approaches, Renewable and Sustainable Energy Reviews, 226 (2026) 116226.

[13] Pérez-Gallego D., Gonzalez-Ayala J., Medina A., Hernández A.C., Performance of packed-bed systems and coupling with brayton cycles, in: Proceedings of the 37th International Conference on Efficiency, Cost, Optimization, Simulation and Environmental Impact of Energy Systems (ECOS 2024), Rhodes, Greece, 2024.

[14] Wang L., Lin X., Zhang H., Peng L., Chen H., Brayton-cycle-based pumped heat electricity storage with innovative operation mode of thermal energy storage array, Applied Energy, 291 (2021) 116821.

[15] Ameen M.T., Ma Z., Smallbone A., Norman R., Roskilly A.P., Demonstration system of pumped heat energy storage (PHES) and its round-trip efficiency, Applied Energy, 333 (2023) 120580.

[16] Bell I.H., Wronski J., Quoilin S., Lemort V., Pure and pseudo-pure fluid thermophysical property evaluation and the open-source thermophysical property library CoolProp, Industrial & Engineering Chemistry Research, 53 (2014) 2498-2508.

[17] Schumann T.E., Heat transfer: a liquid flowing through a porous prism, Journal of the Franklin Institute; 208 (1929) 405-416.

[18] Liu C., Frate G.F., Ferrari L., Desideri U., Thermal performance of segmented design packed bed systems for high-temperature thermal energy storage, in: Proceedings of the 38th International Conference on Efficiency, Cost, Optimization, Simulation and Environmental Impact of Energy Systems (ECOS 2025), Paris, France, 2025.

[19] Ortega-Fernández I., Zavattoni S.A., Rodríguez-Aseguinolaza J., D'Aguanno B., Barbato M.C., Analysis of an integrated packed bed thermal energy storage system for heat recovery in compressed air energy storage technology, Applied Energy, 205 (2017) 280-293.